Ionics (2018) 24:2555–2563
https://doi.org/10.1007/s11581-017-2399-9

ORIGINAL PAPER

Mesoporous Li_2FeSiO_4/C nanocomposites with enhanced performance synthesized from fumed nano silica

Qingtang Zhang[1] · Chao Yan[1] · Junhong Guo[1] · Xiaomei Wang[1]

Received: 27 October 2017 / Revised: 7 December 2017 / Accepted: 10 December 2017 / Published online: 20 December 2017

Abstract

Mesoporous Li_2FeSiO_4/C nanocomposites (LFS-FNS and LFS-NS) were prepared from fumed nano silica (FNS) and nano silica (NS) through facile solid-state reactions, respectively. XRD analysis indicates that the crystalline structures of LFS-FNS and LFS-NS are indexed to monoclinic Li_2FeSiO_4 of $P2_1$. SEM results prove that the particle size of LFS-FNS and FNS (25~40 nm) is smaller than that of LFS-NS and NS, revealing the particle size of Li_2FeSiO_4/C nanocomposites can be tuned by choosing different silica. TEM further indicates Li_2FeSiO_4 nanoparticles are uniformly dispersed in the amorphous carbon networking of LFS-FNS. Pore structure analysis indicates the external surface areas of LFS-FNS as well as LFS-NS are 51.4 and 36.1 $m^2\ g^{-1}$, indicating the pore properties of mesoporous Li_2FeSiO_4/C nanocomposites can be controlled by using different silica as silicon resource. The reduced particle size and high external surface area shorten the lithium-ion diffusion path and make LFS-FNS possess better electrochemical performance over LFS-NS. The discharge capacity of LFS-FNS is as high as 172 mA h g^{-1} at 0.1 C.

Keywords Fumed nano silica · Li_2FeSiO_4 · Mesoporous materials · Nanostructured materials

Introduction

Nowadays, lithium-ion batteries (LIBs) are one of the most promising electrochemical energy storage devices, due to their merits of relatively high power density, high energy density, low self-discharge, long life, no memory effect, and environmental benignity [1–8]. LIBs have been widely used as the main power supplies for portable electronics, electric vehicles, and energy storage. Cathode materials are the key part of LIBs. They roughly decide the electrochemical performance and cost of LIBs. In order to meet the practical applications for electric vehicles and large-scale energy storage, new cathode materials with high capacity and low cost are greatly required. Recently, Li_2FeSiO_4 attracts more and more attentions because of its low cost owing to the abundant raw materials, high safety through strong Si–O bonding, excellent cycling stability, and theoretically high capacity of 332 mA h g^{-1} by allowing reversibly extraction/insertion of two lithium ions per formula unit [9–14].

However, there are innate drawbacks such as low electronic conductivity and sluggish ionic transport capability [12–15], which obviously result in bad electrochemical behaviors of Li_2FeSiO_4-based cathodes and thereby put an obstacle for the applications of Li_2FeSiO_4 in electric vehicles as well as large-scale energy storage. Various approaches, including morphology tuning [9–11, 16], reduced graphene oxide modification [12, 13], carbon nanotube modification [14, 17, 18], porous nanocomposites preparations [15, 19–22], and heterogeneous metal doping [23–30], have been developed to overcome these drawbacks of Li_2FeSiO_4-based cathodes. Among those different approaches, porous nanocomposite preparations have been intensively focused because conductive carbon can enhance the electronic conductivity and porous structure can improve the ionic transport capability. As a result, the electronic and ionic transport capabilities of Li_2FeSiO_4 cathode are well enhanced simultaneously. Till now, different kinds of porous Li_2FeSiO_4/C nanocomposites have been successfully prepared and investigated. For instance, L. Zhang et al. prepared 3D porous Li_2FeSiO_4/C through hydrothermal synthesis followed by carbon nanopainting and the sample delivers a capacity of 167 mA h g^{-1} at 0.1 C [19]. H. Qiu

✉ Xiaomei Wang
wxmei06@163.com

[1] State Key Laboratory of Advanced Processing and Recycling of Non-ferrous Metals, School of Petrochemical Engineering, Lanzhou University of Technology, Lanzhou 730050, China

et al. synthesized mesoporous Li_2FeSiO_4@ordered mesoporous carbon with a capacity of 160 mA h g^{-1} at 0.1 C via a sol-gel method followed by heat treating [20]. Z. Zheng et al. fabricated porous Li_2FeSiO_4/C nanocomposites with a capacity of 176.8 mA h g^{-1} at 0.5 C by the similar method [22]. In a word, these porous Li_2FeSiO_4/C nanocomposites are usually fabricated by complicated multistep process. Usually, the first step is to prepare Li_2FeSiO_4 precursors in the present of surfactant and the second step is to calcine the obtained precursors.

As a facile fabrication method, solid-state reaction is widely used to prepare polycrystalline solids from a mixture of solid starting materials. It is also employed to fabricate different cathode materials for LIBs [12, 18, 31–34]. Pore structure may be destroyed during the ball-milling of solid starting materials or the high-temperature sintering. However, silica possesses high thermal and mechanical stability. We have successfully controlled the particle size of Li_2FeSiO_4/C nanocomposites by employing nano silica with different particle size via solid-state reaction [32]. It can be expected that silica partly keep its porous structure during the ball-milling and high-temperature sintering. So, it is possible to obtain porous Li_2FeSiO_4/C nanocomposites from fumed nano silica (FNS) with high specific area. In this paper, mesoporous Li_2FeSiO_4/C nanocomposites were successfully fabricated from nano fumed silica through a facile solid-state reaction. For comparison, their control was also prepared from nano silica (NS) under the same conditions. Our attempts provide a simple new route to tune the porous structure of Li_2FeSiO_4-based cathode materials through solid-state reactions. Exploring the structure and electrochemical performance of these mesoporous Li_2FeSiO_4/C nanocomposites is an interesting issue for the cathodes of LIBs.

Experimental

Mesoporous Li_2FeSiO_4/C nanocomposites were fabricated by a facile solid-state reaction from the mixture of Li_2CO_3, $FeC_2O_4{\cdot}2H_2O$, FNS (Aladdin, Shanghai), and poly(vinylpyrrolidone) (PVP). All the reagents are analytical grade without any purification. In a typical synthesis, 0.015 mol Li_2CO_3, 0.015 mol $FeC_2O_4{\cdot}2H_2O$, 0.015 mol nano fumed silica, and 1.57 g PVP were put into a stainless steel tank with 20 ml ethanol and mechanically ball-milled for 100 min. Here, PVP is used as a carbon source. The resulting mixture was dried at 65 °C in a vacuum oven for 6 h to obtain the dry precursor. The dry precursor was firstly kept at 400 °C for pre-carbonization of PVP and then calcined at 700 °C for 6 h in the flow of argon gas to fabricate the mesoporous Li_2FeSiO_4/C nanocomposites. The mesoporous Li_2FeSiO_4/C nanocomposites were designated as LFS-FNS. In order to compare, the counterpart was also prepared from a mixture of Li_2CO_3, $FeC_2O_4{\cdot}2H_2O$, NS (Aladdin, Shanghai), and PVP under the same conditions. The counterpart was designated as LFS-NS.

The crystalline structure of the two samples was determined by powder X-ray diffraction (XRD; Rigaku RINT2000) with a Cu Kα radiation ($\lambda = 0.154$ nm). The carbon contents of the two samples were further ascertained by an elemental analysis instrument (Elementar Analysensysteme GmbH). The micro morphologies of FNS, NS, LFS-FNS, LFS-NS, and cycled Li_2FeSiO_4/C cathodes were investigated by a scanning electron microscope (SEM; JSM6701F, JEOL). The micro morphologies of LFS-FNS were further determined by transmission electron microscope (TEM; JEOL JSM2010F). The porous structure of FNS, NS, LFS-FNS, and LFS-NS was determined by nitrogen adsorption/desorption analysis at − 196 °C using a micromeritics ASAP 2020 apparatus.

Mesoporous Li_2FeSiO_4/C nanocomposites (LFS-FNS and LFS-NS), Super P carbon black (Timcal), and aqueous LA132 binder (Chengdu Indigo power sources Co., Ltd.) in a weight ratio of 8:1:1 were mixed together in the de-ionized water to form a homogenous slurry. The slurry in each case was coated onto an aluminum foil and the coated electrodes were dried at 100 °C for 12 h in a vacuum. The mass loading of active materials in the electrodes was about 2.0 mg cm^{-2}. One mole per liter $LiPF_6$ in a mixture of ethyl-methyl carbonate:ethylene carbonate:dimethyl carbonate with a volume ratio of 1:1:1 was used as the electrolyte. The CR2032 coin cells containing lithium flake, electrolyte, porous Li_2FeSiO_4/C nanocomposite electrodes, and celgard 2400 separator were assembled in an argon-filled glove box. Then, the cells were charge-discharged at a constant current between 1.5 and 4.8 V utilizing a LAND CT2001A battery testing system (Wuhan LAND Electronics Co., Ltd.). The cyclic voltammetry (CV) of the fresh cells was recorded on a ZF100 electrochemical workstation (Shanghai Zhengfang Electronics Co., Ltd.) with different scan rates. The electrochemical impedance spectra (EIS) were performed at a CHI660E electrochemical workstation (Shanghai Chenhua Instruments Co., China). The EIS measurements were undertaken with an amplitude of 5 mV in a frequency range from 0.01 Hz to 100 kHz.

Results and discussion

Figure 1 is the XRD patterns of LFS-FNS and LFS-NS. Similar peaks are observed for the two samples. The peaks at (101), (111), (− 202), (− 103), (020), (013), (220) (222), (− 511), (032), and (521) are clearly observed for the two samples. All these peaks can be well indexed to the monoclinic Li_2FeSiO_4 with a space group of $P2_1$ [14, 15, 20–26], indicating that both samples have periodically opposite corner-shared SiO_4 and FeO_4 tetrahedral [35]. Few Fe_3O_4 impurities are also observed in both samples. These phenomena are commonly found in the Li_2FeSiO_4/C

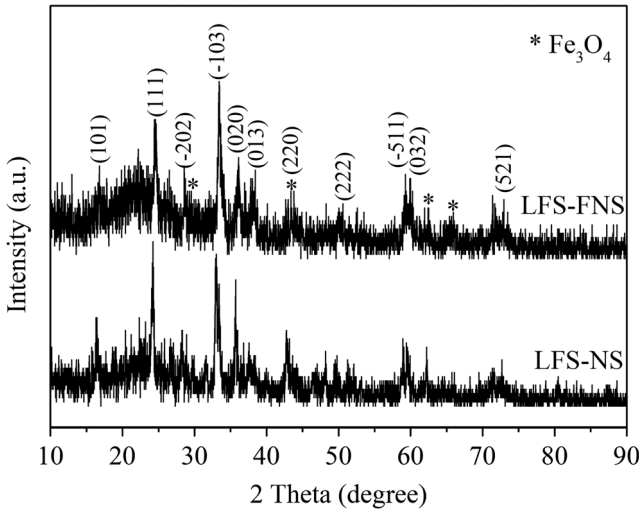

Fig. 1 XRD patterns for LFS-FNS and LFS-NS

nanocomposites synthesized using solid-state reactions [12, 18]. The carbon contents for the two samples are determined by an elemental analysis. The carbon and nitrogen contents for LFS-FNS are 9.8 and 0.5 wt%, while those for LFS-NS are 9.7 and 0.4 wt%. But, no typical peaks of carbon are observed for both samples, indicating the amorphous carbon is in the composites.

SEM images of LFS-FNS, LFS-NS, FNS, and NS are presented in Fig. 2. Seen from the SEM images with low magnification (Fig. 2a, d), the morphologies of both samples are similar and many void spaces are observed for LFS-FNS and LFS-NS. The SEM images with high magnification are shown as Fig. 2b, e. The sphere-like primary nanoparticles are observed for LFS-FNS and LFS-NS. Figure 2b insert is the particle size distribution of LFS-FNS, which is mainly ranging from 25 to 40 nm. While for LFS-NS (Fig. 2e insert), the particle size distribution is mainly ranging from 35 to 55 nm. The particle size of LFS-FNS is clearly smaller than that of LFS-NS. Usually, solid-state reaction results in larger particle size, but the particles of LFS-FNS and LFS-NS are in nano sized. It may be attributed to the PVP-derived carbon, which efficiently suppresses the growth of Li_2FeSiO_4 particles. Reduced particle size can shorten the lithium-ion diffusion path and then enhance the electrochemical performance. In addition, as shown in Fig. 2b, e, the degree of aggregation of LFS-FNS is obviously lower than that of LFS-NS. The primary nanoparticles of LFS-NS tend to form large aggregations. Figure 2c, f is the SEM images for FNS and NS, respectively. Figure 2c insert indicates that the particle size distribution of FNS is mainly in the range of 25–40 nm, which is basically consistent with that of LFS-FNS, while that for NS is mainly in the range of 40–55 nm (Fig. 2f insert). The particle size of NS is accord with that of LFS-NS. These indicate that the particle size of Li_2FeSiO_4/C can be controlled by the particle size of silica.

LFS-FNS were chosen to further investigate the micro morphology with TEM. As shown in Fig. 3a, Li_2FeSiO_4 nanoparticles are uniformly dispersed in the amorphous carbon networking. It is difficult to distinguish the particle size of carbon from TEM image. Carbon networking is very valid in enhancing the electronic conductivity of LFS-FNS and then improving their electrochemical performance. The particle size distribution is shown in Fig. 3a insert. The particle sizes of Li_2FeSiO_4 nanoparticles for LFS-FNS are ranging from 20 to 55 nm, mainly from 25 to 35 nm. It is consistent with the particle size distributions from SEM results. Figure 3b is the high-resolution TEM image of LFS-FNS. Carbon layers are clearly observed at the fringe of Li_2FeSiO_4 crystal. The carbon layers can effectively prevent the Li_2FeSiO_4 crystals from growing.

In order to understand the relationship of porous properties between nano silica and mesoporous Li_2FeSiO_4/C nanocomposites, FNS, NS, LFS-FNS, and LFS-NS were characterized by N_2 adsorption-desorption. Figure 4a is the N_2 adsorption/desorption isotherms of FNS and NS. The isotherms are typical IV isotherms with a H4 hysteresis loop in the range of 0.8–1.0 P/P_0. It indicates FNS and NS are typical mesoporous materials. The total Brunauer-Emmet-Teller (BET) surface areas for FNS and NS are 263.4 and 140.1 $m^2\ g^{-1}$, respectively. According to the *t*-plot method, the external surface areas (including mesopores and macropores) of LFS-FNS and LFS-NS are 240.5 and 110.3 $m^2\ g^{-1}$. Figure 4b is the pore size distributions of FNS and NS calculated by Barrett-Joyner-Halenda (BJH) method. Compared to NS, FNS has much higher pore surface area and clearly broader pore size distributions. As shown in Fig. 4c, LFS-FNS and LFS-NS both exhibit typical IV isotherms with a H4 hysteresis loop in the range of 0.5–1.0 P/P_0, indicating the typical mesoporous characters for both LFS-FNS and LFS-NS. The total BET surface area of LFS-FNS is 54.9 $m^2\ g^{-1}$, while that of LFS-NS is 42.6 $m^2\ g^{-1}$. According to the *t*-plot method, the external surface areas of LFS-FNS and LFS-NS are 51.4 and 36.1 $m^2\ g^{-1}$. Compared with the surface area of FNS and NS, the BET surface area and external surface area of LFS-FNS and LFS-NS are distinctly decreased. As shown in Fig. 4d, the pore size distributions of LFS-FNS and LFS-NS are very similar. The pore sizes mainly locate around 3 and 70 nm. Despite of the pores larger than 80 nm, the pore surface areas of LFS-FNS are clearly higher than those of LFS-NS. Seen from Fig.4b, d, the pore size distributions of FNS, NS, LFS-FNS, and LFS-NS are similar to some extent. The pore sizes of the four samples mainly range from 3 to 70 nm. These phenomena indicate that pore properties of mesoporous Li_2FeSiO_4/C nanocomposites can be well controlled by using different silica as silicon resource. As it is well known, the mesopores can offer channels for fast lithium-ion transport, which greatly improve the electrochemical properties of electrode materials. LFS-FNS should deliver much better

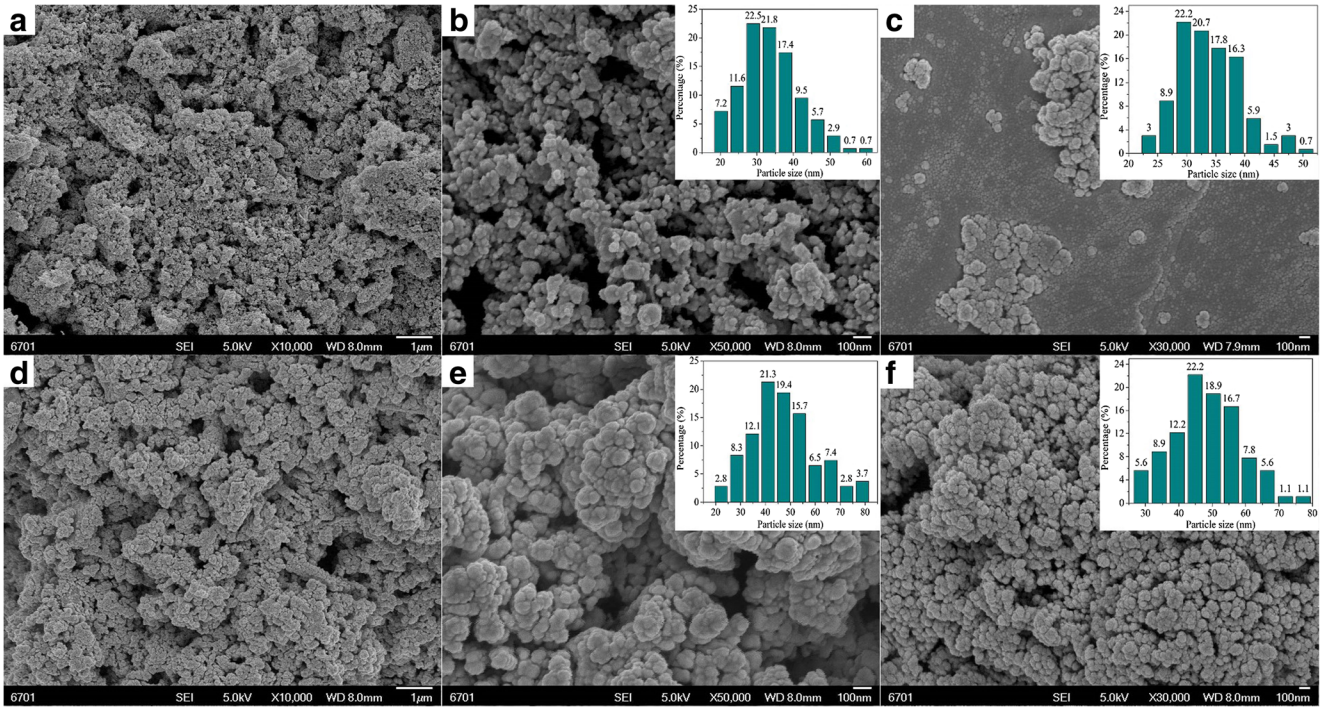

Fig. 2 SEM images of the samples: **a**, **b** LFS-FNS; **c** FNS; **d**, **e** LFS-NS; and **f** NS. Particle size distributions for **b** (insert) LFS-FNS, **c** (insert) FNS, **e** (insert) LFS-NS, and **f** (insert) NS

electrochemical performance over LFS-NS because LFS-FNS possess enriched mesopores.

The fresh cells containing the two samples are further measured by CV in the voltage window of 1.5–4.8 V with a scan rate of 0.1 mV s^{-1}. The CV curves are present as Fig. 5. Figure 5a is the first CV scans of the two samples. LFS-FNS have an anodic peak at 3.20 V and a cathodic peak at 2.57 V. LFS-NS have an anodic peak at 3.36 V and a cathodic peak at 2.50 V. The anodic peak corresponds to the oxidation of Fe^{2+} to Fe^{3+} and the cathodic peak corresponds to the reduction of Fe^{3+} to Fe^{2+}. The difference between the anodic and cathodic peak of LFS-FNS is 0.63 V, lower than that of LFS-NS 0.86 V. This indicates that LFS-FNS has a weaker polarization due to the much more mesopores of LFS-FNS allowing fast ion transport. Figure 5b is the third CV scan of the two samples. The anodic peaks of LFS-FNS and LFS-NS both reduce to 3.10 and 3.24 V, respectively. The cathodic peaks of the two samples both increase to 2.58 V. These indicate the polarization becomes smaller during the repeated CV scans. Figure 5c is the initial charge/discharge voltage curve of LFS-FNS and LFS-NS. Obviously, the charge and discharge capacities of LFS-FNS are much higher than those of LFS-NS. The charge and discharge capacities for LFS-FNS at 0.1 C are

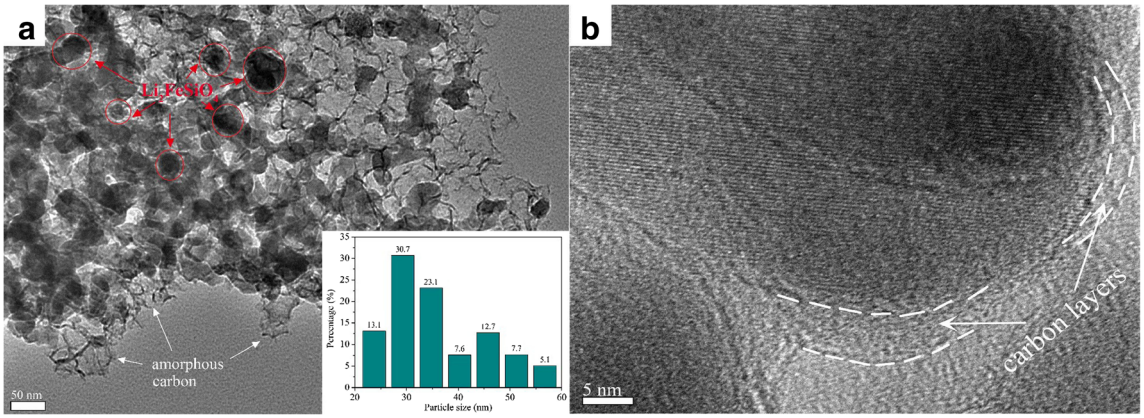

Fig. 3 TEM image for LFS-FNS

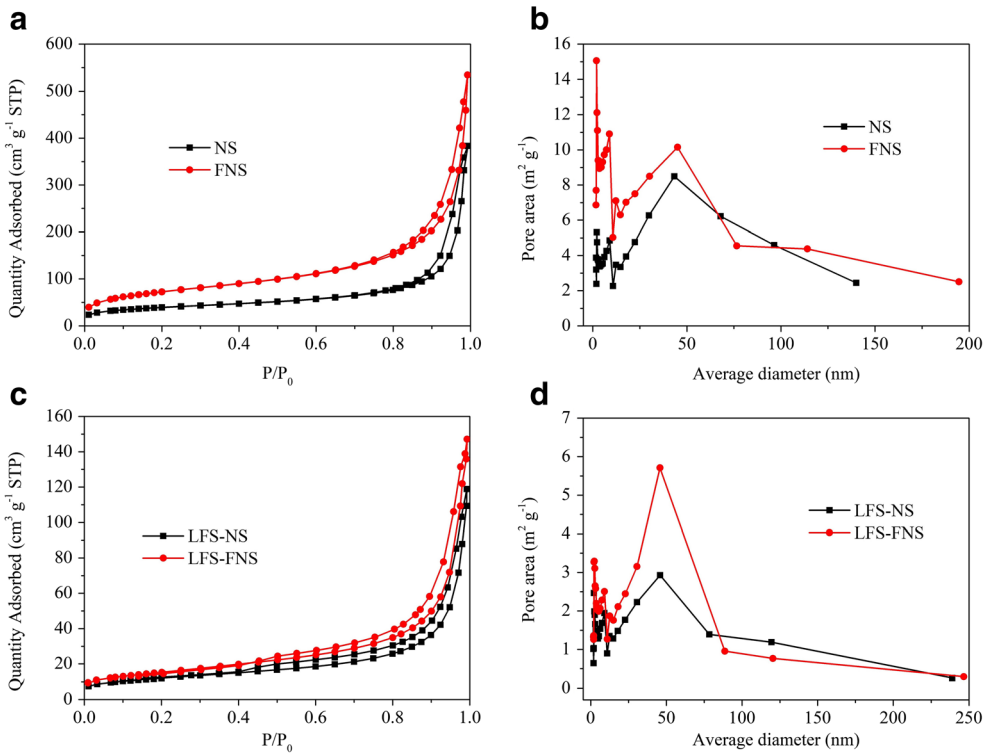

Fig. 4 **a**, **c** Nitrogen adsorption-desorption isotherms of FNS, NS, LFS-FNS, and LFS-NS. **b**, **d** Pore size distribution of FNS, NS, LFS-FNS, and LFS-NS

180 and 172 mA h g^{-1}, respectively. As illustrated in Table 1, the discharge capacity of LFS-FNS is higher than that of most L_2FeSiO_4/C samples, while the charge and discharge capacities for LFS-NS are143 and 133 mA h g^{-1}, respectively. Figure 5d shows the charge/discharge voltage curve of the third cycle. The charge and discharge capacities of LFS-FNS are also much higher than those of LFS-NS. In addition, LFS-FNS show a lower charge voltage plateau and higher discharge voltage plateau compared to LFS-NS. The results are in good agreement with the CV tests.

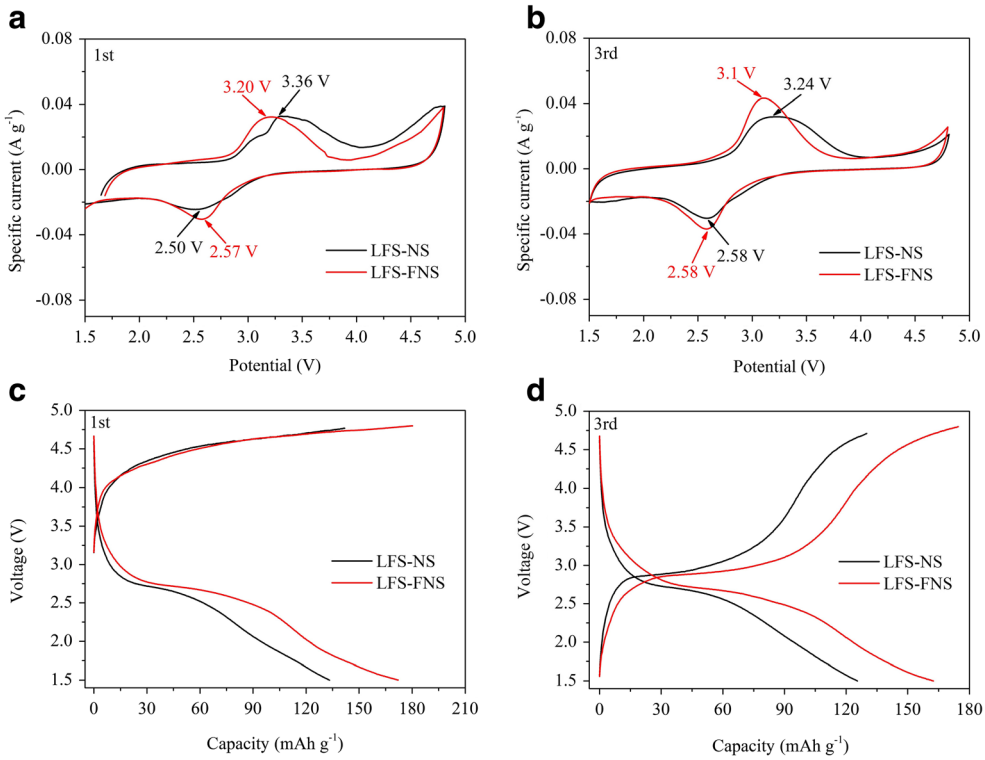

Fig. 5 Charge-discharge voltage curves for LFS-FNS and LFS-NS: **a** first cycle and **b** third cycle. CV curves of at a scan rate of 0.1 mV s^{-1}: **c** first cycle and **d** third cycle

Table 1 Comparison of the discharge capacity of Li_2FeSiO_4/C at low current density

Samples	Current density	Discharge capacity (mA h g^{-1})	References
LFS-FNS	0.1 C	172	This work
3D porous hierarchical Li_2FeSiO_4/C	0.1 C	163	[19]
$Li_2Fe_{0.97}Mg_{0.03}SiO_4$/C	10 mA g^{-1}	153.2	[25]
Yttrium-doped Li_2FeSiO_4/C	0.2 C	156	[26]
$Li_2Fe_{0.9}Mn_{0.1}SiO_4$/C	C/16	151.4	[28]
$Li_2Fe_{0.97}Zn_{0.03}SiO_4$/C	10 mA g^{-1}	158	[27]
Li_2FeSiO_4/C	0.1 C	150	[33]
Li_2FeSiO_4/C	10 mA g^{-1}	129	[34]

Figure 6a shows the specific capacity for LFS-FNS and LFS-NS at different current rates from 0.1 to 3 C (1 C = 166 mA h g^{-1}). The specific capacities of both samples decrease with the current rate increasing. The specific capacities of LFS-FNS are higher than those of LFS-NS at every rate. For instance, LFS-FNS deliver discharge capacities of 172, 143, 118, 99, 83, and 79 mA h g^{-1} at the rates of 0.1, 0.2, 0.5, 1, 2, and 3 C. LFS-NS deliver discharge capacities of 133, 115, 96, 82, 71, and 63 mA h g^{-1}. When restored to 0.1 C, the discharge capacities of LFS-FNS and LFS-NS are 152 and 121 mA h g^{-1}. The excellent rate performance of LFS-FNS is attributed to their high mesoporous specific area and carbon coating, which have the following merits [36, 37]: (i) The carbon coating hinders the Li_2FeSiO_4 crystals growing, which allows high electronic and ionic conductivity and (ii) the enriched mesopores facilitate the electrolyte to soak in and allow fast transport of lithium ions. The two Li_2FeSiO_4/C samples are charge-discharged at 1 C for 90 cycles and the results are shown in Fig. 6b. The first discharge capacity of LFS-FNS is 109 mA h g^{-1}, and that for LFS-NS is 90 mA h g^{-1}. The discharge capacity of LFS-FNS after 90 charge-discharge cycles is 95 mA h g^{-1} and that for LFS-NS is 79 mA h g^{-1}. Therefore, the capacity retention ratios of LFS-FNS and LFS-NS are 87.2 and 87.8%. The value of LFS-FNS is very close to that of LFS-NS. But LFS-NS has a much higher specific capacity.

The Nyquist plots of the fresh coin cells loaded with LFS-FNS and LFS-NS are fitted with the equivalent circuit (Fig. 7a insert). As shown in Fig. 7a, both plots are composed of one semicircle and a line in the low-frequency region. Generally, the intercept at the Z' axis in the high frequency is the ohmic resistance of the electrolyte (R_e). R_e of LFS-FNS is 2.8 Ω and that of LFS-NS is 7.2 Ω. The semicircle in the middle frequency range refers to the charge transfer resistance (R_{ct}). The R_{ct} of LFS-FNS is 246.1 Ω and that of LFS-NS is 312.4 Ω. Re and R_{ct} of LFS-FNS are much lower than those of LFS-NS. The inclined line in the low frequency reveals the Warburg impedance (Z_w), which is associating the lithium-ion diffusion ability of the sample. Figure 7b shows the linear relationship between Z' and reciprocal square root of frequency ($\omega^{-0.5}$) in the low-frequency region. The lithium-ion diffusion coefficient (D_{Li+}) could be calculated from the sloping line according to the following Eqs. (1 and 2) [26, 27, 29]:

$$D_{Li+} = \frac{R^2T^2}{2A^2n^4F^4C^2\sigma^2} \quad (1)$$

$$Z' = R_e + R_{ct} + \sigma\omega^{-1/2} \quad (2)$$

where R is gas constant, T is the absolute temperature, A is the surface area of the electrode (1.13 cm^2), n is the number of transferred electrons, F is the Faraday constant and C is the

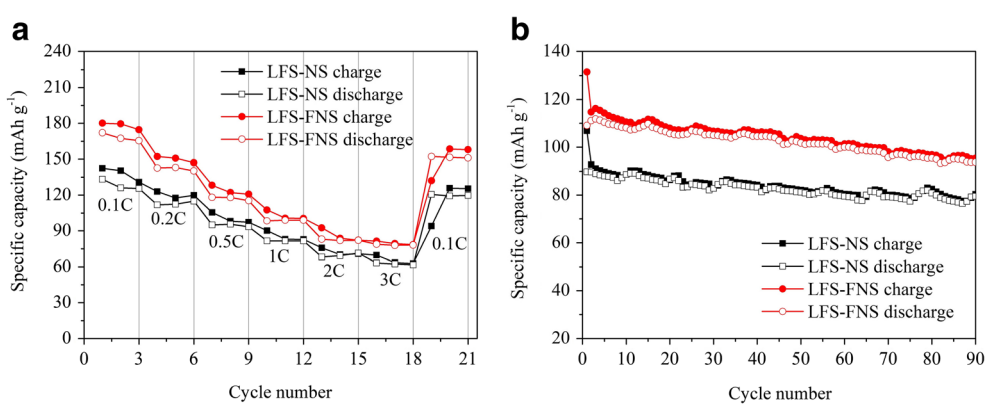

Fig. 6 **a** Rate performance of LFS-FNS and LFS-NS. **b** Cycling performance of LFS-FNS and LFS-NS at a current rate of 1 C

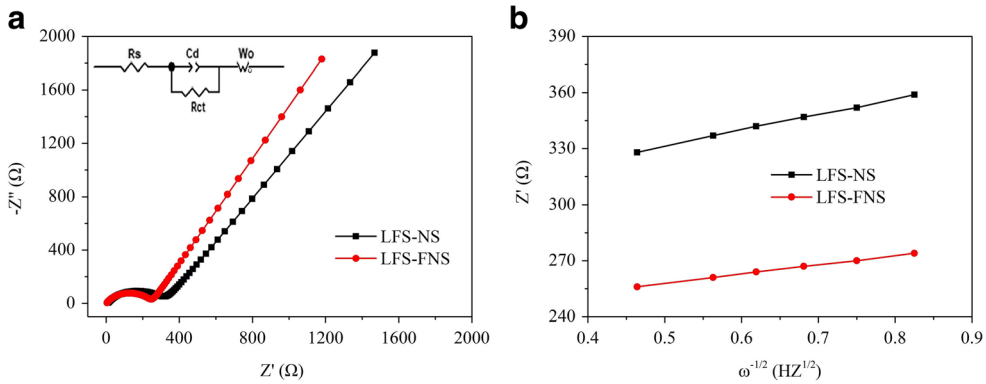

Fig. 7 **a** Nyquist plots of the LFS-FNS and LFS-NS. **b** Linear relationship between Z' and $\omega^{-0.5}$ in the low-frequency region

bulk concentration of lithium ions, Z' is the real impedance, σ is Warburg impedance coefficient obtained from the Eq. (2), and ω is frequency in the low range. The D_{Li+} of LFS-FNS and LFS-NS is 1.01×10^{-14} and 2.46×10^{-15} cm^2 s^{-1}, respectively. D_{Li+} of LFS-FNS is much higher than that of LFS-NS and also higher than that Mg-doped Li_2FeSiO_4/C [24]. The higher lithium-ion diffusion coefficient should be attributed to the smaller nanoparticle size and larger mesoporous surface area of LFS-FNS. The smaller particle size can shorten the lithium-ion diffusion path. The mesopores can adsorb and retain electrolyte, which allows fast lithium ion penetration. As a result, LFS-FNS exhibit lithium-ion diffusion coefficient, low R_e, and low R_{ct}.

Figure 8 is the SEM images for LFS-FNS cathode and LFS-NS cathode after 100 charge/discharge cycles at 1 C. The sphere-like primary nanoparticles are also observed for both LFS-FNS cathode and LFS-NS cathode. As shown in Fig. 8a, nanoparticles with sizes of 30~50 nm are observed for LFS-FNS cathode. The particle size of LFS-FNS cathode is only slightly larger than that of LFS-FNS. While for LFS-NS (Fig. 8b), nanoparticles with sizes of 45~65 nm are observed for LFS-NS cathode. In addition, the degree of aggregation of LFS-FNS cathode is obviously lower than that of LFS-NS cathode. These results show that the cycled electrode material almost possesses original morphology. The weak structural and morphology changes ensure both cathodes possess stable cyclic performance.

Conclusion

In summary, mesoporous Li_2FeSiO_4/C nanocomposites with different pore properties (LFS-FNS and LFS-NS) were successfully prepared from nano fumed silica and nano silica through facile solid-state reactions. XRD analysis reveals LFS-FNS and LFS-NS are crystals with monoclinic Li_2FeSiO_4. SEM results indicate that the particle size of LFS-FNS and FNS is in the range of 20–40 nm, which is smaller than that of LFS-NS and NS. It indicates that particle size of Li_2FeSiO_4/C can be controlled by the particle size of silica. TEM further indicates Li_2FeSiO_4 nanoparticles are uniformly dispersed in the amorphous carbon networking of LFS-FNS. Pore structure analysis indicates the external surface areas of LFS-FNS and LFS-NS are 51.4 and 36.1 m^2 g^{-1}. It reveals the pore properties of Li_2FeSiO_4/C nanocomposites can be tuned by choosing different silica. The carbon networking, reduced particle size, and high external surface area make LFS-FNS possess better electrochemical performance over LFS-NS. The discharge capacity of LFS-FNS at 0.1 C reaches

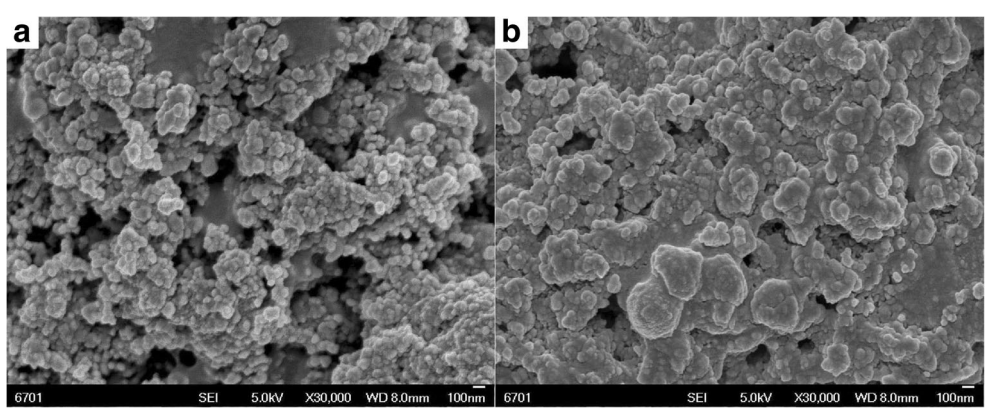

Fig. 8 SEM images for LFS-FNS cathode (**a**) and LFS-NS cathode (**b**) after 100 charge/discharge cycles at 1 C

to 172 mA h g^{-1}. In addition, LFS has better rate performance, higher lithium diffusion coefficient, lower R_e, and lower R_{ct}.

Funding information This research was supported by the Gansu Provincial Science Fund (1606RJZA180) and the National Nature Science Foundation of China (No. 21466020).

References

1. Sun Y, Liu N, Cui Y (2016) Promises and challenges of nanomaterials for lithium-based rechargeable batteries. Nature Energy 1(7):16071–16082. https://doi.org/10.1038/nenergy.2016.71
2. Zhang Q, Zhao Y, Su C, Li M (2011) Nano micro lithium transitionmetal (Fe Mn, Co and Ni) silicate cathode materials for lithium ion batteries. Recent Pat Nanothechnol 5(3):225–233. https://doi.org/10.2174/1872210511105030225
3. Marom R, Amalraj SF, Leifer N, Jacob D, Aurbach D (2011) A review of advanced and practical lithium battery materials. J Mater Chem 21(27):9938–9954. https://doi.org/10.1039/c0jm04225k
4. Zhang Q, Xie X, Fan W, Wang X (2016) Lithium polyacrylate-coated $LiMn_2O_4$ cathode materials with excellent performance for lithium ion batteries. Ionics 22(12):2273–2280. https://doi.org/10.1007/s11581-016-1766-2
5. Larcher D, Tarascon JM (2015) Towards greener and more sustainable batteries for electrical energy storage. Nat Chem 7:19–29. https://doi.org/10.1038/nchem.2085
6. Ni J, Jiang Y, Bi X, Li L, Lu J (2017) Lithium iron orthosilicate cathode: progress and perspectives. ACS Energy Lett 2(8):1771–1781. https://doi.org/10.1021/acsenergylett.7b00452
7. Masquelier C, Croguennec L (2013) Polyanionic (phosphates, silicates, sulfates) frameworks as electrode materials for rechargeable Li (or Na) batteries. Chem Rev 113(8):6552–6591. https://doi.org/10.1021/cr3001862
8. Ni J, Zhang L, Fu S, Savilov SV, Aldoshin SM, Lu L (2015) A review on integrating nano-carbons into polyanion phosphates and silicates for rechargeable lithium batteries. Carbon 92:15–25
9. Yi L, Wang G, Bai Y, Liu M, Wang X, Liu M, Wang X (2017) The effects of morphology and size on performances of Li_2FeSiO_4/C cathode materials. J Alloys Compd 721:683–690. https://doi.org/10.1016/j.jallcom.2017.06.059
10. Qu L, Fang SH, Yang L, Hirano SI (2012) Li_2FeSiO_4/C cathode material synthesized by template-assisted sol-gel process with Fe_2O_3 microsphere. J Power Sources 217:243–247. https://doi.org/10.1016/j.jpowsour.2012.05.093
11. Yang J, Kang X, He D, Peng T, Hu L, Mu S (2013) Hierarchical shuttle-like Li_2FeSiO_4 as a highly efficient cathode material for lithium-ion batteries. J Power Sources 242:171–178. https://doi.org/10.1016/j.jpowsour.2013.05.088
12. Wang X, Qing C, Zhang Q, Fan W, Huang X, Yang B, Cui J (2014) Facile synthesis and enhanced electrochemical performance of Li_2FeSiO_4/C/reduced graphene oxide nanocomposites. Electrochim Acta 134:371–376. https://doi.org/10.1016/j.electacta.2014.04.170
13. Zhu H, Wu X, Zan L, Zhang Y (2014) Superior electrochemical capability of Li_2FeSiO_4/C/G composite as cathode material for Li-ion batteries. Electrochim Acta 117:34–40. https://doi.org/10.1016/j.electacta.2013.11.089
14. Peng G, Zhang LL, Yang XL, Duan S, Liang G, Huang YH (2013) Enhanced electrochemical performance of multi-walled carbon nanotubes modified Li_2FeSiO_4/C cathode material for lithium-ion batteries. J Alloys Compd 570:1–6. https://doi.org/10.1016/j.jallcom.2013.03.136
15. Chen Z, Qiu S, Cao Y, Qian J, Ai X, Xie K, Hong X, Yang H (2013) Hierarchical porous Li_2FeSiO_4/C composite with 2 Li storage capacity and long cycle stability for advanced Li-ion batteries. J Mater Chem A 1(16):4988–4992. https://doi.org/10.1039/c3ta00611e
16. Devaraju MK, Tomai T, Honma I (2013) Supercritical hydrothermal synthesis of rod like Li_2FeSiO_4 particles for cathode application in lithium ion batteries. Electrochim Acta 109:75–81. https://doi.org/10.1016/j.electacta.2013.07.056
17. Zhao Y, Li J, Wang N, Wu C, Ding Y, Guan L (2012) In situ generation of Li_2FeSiO_4 coating on MWNT as a high rate cathode material for lithium ion batteries. J Mater Chem 22(36):18797–18800. https://doi.org/10.1039/c2jm33855f
18. Huang X, Li X, Wang H, Pan Z, Qu M, Yu Z (2010) Synthesis and electrochemical performance of Li_2FeSiO_4/carbon/carbon nanotubes for lithium ion battery. Electrochim Acta 55(24):7362–7366. https://doi.org/10.1016/j.electacta.2010.07.036
19. Zhang L, Ni J, Wang W, Guo J, Li L (2015) 3D porous hierarchical Li_2FeSiO_4/C for rechargeable lithium batteries. J Mater Chem A 3(22):11782–11786. https://doi.org/10.1039/C5TA02433A
20. Qiu H, Zhu K, Li H, Li T, Zhang T, Yue H, Wei Y, Du F, Wang C, Chen G, Zhang D (2015) Mesoporous Li_2FeSiO_4@ordered mesoporous carbon composites cathode material for lithium-ion batteries. Carbon 87:365–373. https://doi.org/10.1016/j.carbon.2015.02.056
21. Ding Z, Liu J, Ji R, Zeng X, Yang S, Pan A, Ivey DG, Wei W (2016) Three-dimensionally ordered macroporous Li_2FeSiO_4/C composite as a high performance cathode for advanced lithium ion batteries. J Power Sources 329:297–304. https://doi.org/10.1016/j.jpowsour.2016.08.091
22. Zheng Z, Wang Y, Zhang A, Zhang T, Cheng F, Tao Z, Chen J (2012) Porous Li_2FeSiO_4/C nanocomposite as the cathode material of lithium-ion batteries. J Power Sources 198:229–235. https://doi.org/10.1016/j.jpowsour.2011.09.066
23. Ren Y, Lu P, Huang X, Ding J, Wang H, Zhou S, Chen Y, Ding X (2016) Spherical $Li_{1.95}Na_{0.05}FeSiO_4$/C composite as nanoporous cathode material exhibiting high rate capability. Mater Lett 173:207–210. https://doi.org/10.1016/j.matlet.2016.03.048
24. Qu L, Luo D, Fang S, Liu Y, Yang L, Hirano S, Yang CC (2016) Mg-doped Li_2FeSiO_4/C as high-performance cathode material for lithium-ion battery. J Power Sources 307:69–76. https://doi.org/10.1016/j.jpowsour.2015.12.137
25. Zhang S, Deng C, BL F, Yang SY, Ma L (2010) Doping effects of magnesium on the electrochemical performance of Li_2FeSiO_4 for lithium ion batteries. J Electroanal Chem 644(2):150–154. https://doi.org/10.1016/j.jelechem.2009.11.035
26. Qiu H, Yue H, Zhang T, Ju Y, Zhang Y, Guo Z, Wang C, Chen G, Wei Y, Zhang D (2016) Enhanced electrochemical performance of Li_2FeSiO_4/C positive electrodes for lithium-ion batteries via yttrium doping. Electrochim Acta 188:636–644. https://doi.org/10.1016/j.electacta.2015.12.042
27. Deng C, Zhang S, Yang SY, BL F, Ma L (2011) Synthesis and characterization of $Li_2Fe_{0.97}M_{0.03}SiO_4$ (M=Zn^{2+}, Cu^{2+}, Ni^{2+}) cathode materials for lithium ion batteries. J Power Sources 196(1):386–392. https://doi.org/10.1016/j.jpowsour.2010.06.064
28. Guo HJ, Cao X, Li XQ, Li LM, Li XH, Wang ZX, Peng W, Li Q (2010) Optimum synthesis of $Li_2Fe_{1-x}Mn_xSiO_4$/C cathode for lithium ion batteries. Electrochim Acta 55(27):8036–8042. https://doi.org/10.1016/j.electacta.2010.03.001
29. Yi L, Wang X, Wang G, Bai Y, Liu M, Wang X, Yu R (2016) Improved electrochemical performance of spherical Li_2FeSiO_4/C cathode materials via Mn doping for lithium-ion batteries. Electrochim Acta 222:1354–1364. https://doi.org/10.1016/j.electacta.2016.11.111
30. Zhang LL, Duan S, Yang XL, Liang G, Huang YH, Cao XZ, Yang J, Li M, Croft MC, Lewis C (2015) Insight into cobalt-doping in Li_2FeSiO_4 cathode material for lithium-ion battery. J Power

Sources 274:194–202. https://doi.org/10.1016/j.jpowsour.2014.10.048

31. Liu Q, Yu L, Wang H (2009) Preparation of $LiMn_2O_4$ with an enhanced performance by mixed liquid and mechanical activations. J Alloys Compd 486(1-2):886–889. https://doi.org/10.1016/j.jallcom.2009.07.087
32. Cui J, Qing C, Zhang Q, Su C, Wang X, Yang B, Huang X (2014) Effect of the particle size on the electrochemical performance of nano-Li_2FeSiO_4/C composites. Ionics 20(1):23–28. https://doi.org/10.1007/s11581-013-0965-3
33. Zuo P, Wang T, Cheng G, Cheng X, Du C, Yin G (2012) Effects of carbon on the structure and electrochemical performance of Li_2FeSiO_4 cathode materials for lithium-ion batteries. RSC Adv 2(17):6994–6998. https://doi.org/10.1039/c2ra20552a
34. Chen W, Lan M, Zhu D, Wang C, Xue S, Yang C, Li Z, Zhang J, Mi L (2013) Synthesis, characterization and electrochemical performance of Li_2FeSiO_4/C for lithium-ion batteries. RSC Adv 3(2):408–412. https://doi.org/10.1039/C2RA21875E
35. Muraliganth T, Stroukoff KR, Manthiram A (2010) Micro-wave-solvothermal synthesis of nanostructured Li_2MSiO_4/C (M = Mn and Fe) cathodes for lithium-ion batteries. Chem Mater 22(20):5754–5761. https://doi.org/10.1021/cm102058n
36. Jiang Y, Yang Z, Li W, Zeng L, Pan F, Wang M, Wei X, Hu G, Gu L, Yu Y (2015) Nanoconfined carbon-coated $Na_3V_2(PO_4)_3$ particles in mesoporous carbon enabling ultralong cycle life for sodium-ion batteries. Adv Energy Mater 5(10):1402104. https://doi.org/10.1002/aenm.201402104
37. Wang W, Liang H, Zhang L, Savilov SV, Ni J, Li L (2017) Carbon nanotube directed three-dimensional porous Li_2FeSiO_4 composite for lithium batteries. Nano Res 10(1):229–237. https://doi.org/10.1007/s12274-016-1280-x